Petroleum Science 21 (2024) 2273–2286

Contents lists available at ScienceDirect

Petroleum Science

journal homepage: www.keaipublishing.com/en/journals/petroleum-science

Original Paper

Investigations of methane adsorption characteristics on marine-continental transitional shales and gas storage capacity models considering pore evolution

Chen-Gang Lu [a, b], Xian-Ming Xiao [a, *], Zhen-Qian Xue [c], Zhang-Xin Chen [c, d, **], Yin-Tao Dong [e], Yue Feng [a], Gang Li [a]

[a] School of Energy Resources, China University of Geosciences (Beijing), Beijing, 100083, China
[b] School of Civil and Environmental Engineering, Nanyang Technological University, 50 Nanyang Avenue, 639798, Singapore
[c] Chemical and Petroleum Engineering, University of Calgary, Calgary, Alberta, T2N 1N4, Canada
[d] Eastern Institute of Technology (tentative), Ningbo, 315000, Zhejiang, China
[e] CNOOC Research Institute, Beijing, 100028, China

ARTICLE INFO

Article history:
Received 12 July 2023
Received in revised form
9 October 2023
Accepted 31 March 2024
Available online 16 April 2024

Edited by Jie Hao and Teng Zhu

Keywords:
High-pressure methane adsorption
Marine-continental transitional shale gas
Ono-Kondo model
Adsorption thermodynamics
Gas storage capacity model

ABSTRACT

Methane adsorption is a critical assessment of the gas storage capacity (GSC) of shales with geological conditions. Although the related research of marine shales has been well-illustrated, the methane adsorption of marine-continental transitional (MCT) shales is still ambiguous. In this study, a method of combining experimental data with analytical models was used to investigate the methane adsorption characteristics and GSC of MCT shales collected from the Qinshui Basin, China. The Ono-Kondo model was used to fit the adsorption data to obtain the adsorption parameters. Subsequently, the geological model of GSC based on pore evolution was constructed using a representative shale sample with a total organic carbon (TOC) content of 1.71%, and the effects of reservoir pressure coefficient and water saturation on GSC were explored. In experimental results, compared to the composition of the MCT shale, the pore structure dominates the methane adsorption, and meanwhile, the maturity mainly governs the pore structure. Besides, maturity in the middle-eastern region of the Qinshui Basin shows a strong positive correlation with burial depth. The two parameters, micropore pore volume and non-micropore surface area, induce a good fit for the adsorption capacity data of the shale. In simulation results, the depth, pressure coefficient, and water saturation of the shale all affect the GSC. It demonstrates a promising shale gas potential of the MCT shale in a deeper block, especially with low water saturation. Specifically, the economic feasibility of shale gas could be a major consideration for the shale with a depth of <800 m and/or water saturation >60% in the Yushe-Wuxiang area. This study provides a valuable reference for the reservoir evaluation and favorable block search of MCT shale gas.

1. Introduction

Natural gas, a transitional energy resource, demonstrates a crucial role in global carbon reduction, while its consumption and supply should be balanced necessarily. Shale gas is a type of unconventional natural gas and has been highly valued and commercially developed based on its enormous resource potential and low-carbon nature (Abdollahi et al., 2022; EIA, 2022). After the commercial development of marine shale gas, the exploration of marine-continental transitional (MCT) shale gas has received further attention in China in recent years (Dong et al., 2021). MCT shales and marine shales significantly differ in their composition and geological conditions. The former is characterized by type III-IIb organic matter (OM) and rich clay minerals (Lu et al., 2023a), while the latter has type I-IIa OM, a high content of brittle minerals

* Corresponding author. School of Energy Resources, China University of Geosciences (Beijing), Beijing, 100083, China.
** Corresponding author. Chemical and Petroleum Engineering, University of Calgary, Calgary, Alberta, T2N 1N4, Canada.
E-mail addresses: xmxiao@cugb.edu.cn (X.-M. Xiao), zhachen@ucalgary.ca (Z.-X. Chen).

https://doi.org/10.1016/j.petsci.2024.03.027

(quartz and carbonate), and a low content of clay. The methane adsorption of shale is mainly related to the type and maturity of OM, and is also influenced to some extent by clays (Chalmers and Bustin, 2008; Gao et al., 2022; Feng et al., 2023a, 2023b; Lu et al., 2023b). Besides, the MCT shale is much shallower in depth and has lower reservoir pressure than the marine shale in China (Guo et al., 2021). These characteristics of MCT shale will affect its methane adsorption capacity (MAC) and GSC model.

Conventionally, the MAC of a shale can be characterized by a correlation model between the shale composition and high-pressure methane adsorption (HPMA) data (Ji et al., 2015; Yang et al., 2015; Jiang et al., 2022). In such kind of models, the composition is mainly chosen as the contents of total organic carbon (TOC) and clays. However, the models only capture limited characteristic parameters of shales and lack quantitative characterization of information such as OM type and maturity, which leads to poor generalization ability of the models.

The geological model of GSC is an essential basis for shale gas evaluation, and it can conclude the capacities of total gas, adsorbed gas, and free gas (Gasparik et al., 2014; Hu and Mischo, 2020). In constructing a geological GSC model, the description of adsorbed gas models is the most important task. Currently, the methane adsorption models have been widely established. Specifically, the Langmuir model characterizes layer adsorption (Ji et al., 2015; Dang et al., 2017); the SDR (supercritical Dubinin-Radushkevich) and SDA (supercritical Dubinin-Astakhov) models are based on adsorption potential and micropore filling (Sakurovs et al., 2007); the SLD (simplified local density) model is based on gas-solid potential energy (Jiang et al., 2018); and the Ono-Kondo model considers adsorption sites (Zhou et al., 2017a; Hu et al., 2021). Furthermore, modified models (Song et al., 2018; Ren et al., 2022) and composite models (Zhou et al., 2017b; Liu et al., 2022a,b) are also proposed, where the modified models are based on the modification of a single model and the composite models are the combination of two single models. However, the composite models are assumed to have two mechanisms of single-layer adsorption and micropore filling coexisting, and this also means more unknown parameters and the potential for computational ambiguity when fitting finite HPMA data (Zhou et al., 2017b). Although fewer parameters need to be fitted for single models, making them more suitable for calculation, the result is sometimes unreasonable. For example, the Langmuir model often produces anomalous results of adsorbed phase density greater than the liquid methane boiling point density (Tian et al., 2016). The SDR model normally does not follow the Henry's law at low pressure, and the current application of the SDR model to fit variable-temperature adsorption experiment data needs to assume a constant value for parameter D (affinity coefficient). However, D is a thermodynamic parameter related to temperature (Okolo et al., 2019), thus a constant D value cannot accurately predict the methane adsorption under variable-temperature conditions (Pan et al., 2016; Li et al., 2017). The iterative integration in the SLD model dramatically increases the computation complexity (Clarkson and Haghshenas, 2016). As for the Ono-Kondo model, there are no assumptions on the adsorption mechanism, and, the adsorption parameters can be fitted from simple calculation. This advantage of Ono-Kondo model has recently attracted great attention in practical applications (Zhou et al., 2017a; Hu and Mischo, 2020).

The GSC model of a shale is assessed by the extrapolation from variable-temperature HPMA experiment data of limited samples. However, it only considers the GSC of the shale with the same maturity and porosity conditions at different depths, and is more suitable for marine shale reservoirs in southern China, such as the Wufeng-Longmaxi formations whose maturity has no correlation with the current burial depth, with an EqRo (equivalent vitrinite reflectance) range of 2.5–3.0% (Xiao et al., 2015; Wang et al., 2019). The GSC model constructed based on the above conditions shows that the free gas increases with increasing depth. The maturity of MCT shale varies greatly in the Qinshui Basin of China (Su et al., 2005; Hou, 2020; Lu et al., 2023a), and the current depth significantly controls the maturity in the central and eastern parts of the basin (Yin and Guo, 2019; Zhang et al., 2019), thereby affecting the reservoir properties of the shale. In addition, under the influence of in-situ stress, shale pores also decrease with depth, thereby reducing the free gas (Miao et al., 2022). Wang et al. (2013) and Cander (2012) have mentioned the effect of shale porosity on GSC with depth, but no further research has been conducted on the GSC models.

The present study proposes a combined experimental and simulation method to investigate the methane adsorption characteristics and GSC model of MCT shale in the Qinshui Basin, China. The HPMA experiments under different temperature and water conditions are conducted on collected MCT shale samples. The Ono-kondo model is used to fit the experiment data to obtain the adsorption parameters, and a geological GSC model of the shale is established considering the joint constraints of maturity and depth on the shale pores, with the analysis of the influence of reservoir pressure coefficients and water saturation on the geological model. The purpose of this work is to provide a guide to the evaluation and exploration of MCT shale gas in the Qinshui Basin.

2. Material and methods

2.1. Basic information of samples

This study collected nine MCT shale samples from the Taiyuan Formation and Shanxi Formation in the Qingshui Basin of China. These samples represent a series of samples across a maturity range from middle to over-mature stages (R_o = 1.25–3.90%). The geological overview of the Qingshui Basin, sedimentary characteristics of the Shanxi-Taiyuan formations, and basic information about the studied samples were described in a previous publication (Lu et al., 2023a). Table 1 lists some experimental data that are directly relevant to this study, including R_o, TOC content, mineral composition, micropore volume, and non-micropore specific surface area. In this study, the total porosity of the shale samples was also measured using the method suggested by Chalmers et al. (2012).

2.2. The high-pressure methane adsorption

The HPMA experiments were performed using an ISOSORP-HP Static II instrument. All samples were conducted at an experimental temperature of 313.15 K and a pressure range of 0–24 MPa. The detailed experimental procedures were described in the references (Xin et al., 2021).

The TOC content of MCT shales in the Qinshui Basin is generally low, with a main range of 1–2% for the shale samples from the Yushe-Wuxiang area (Zhang et al., 2019). Therefore, this study selected the sample S7 (TOC = 1.71%) for additional methane adsorption experiments at three different temperatures (303.15 K, 333.15 K and 363.15 K) to construct a geological model of GSC variation with depth. In addition, equilibrium water experiments were conducted on S7 (detailed steps can be found in Yang et al. (2016)), and the sample with different water contents was obtained for HPMA experiments (313.15 K) to investigate the effect of water on the geological GSC model. The water content of the sample can be used to calculate the water saturation with Eq. (1).

Table 1
Basic experimental data of MCT shale samples.

Samples	Depth, m	R_o*, %	TOC*, %	Clays*, %	S_{non}*, m^2/g	V_{mic}*, $cm^3/100$ g	V_{total}*, $cm^3/100$ g	Apparent density, g/cm^3	Porosity, %
S1	835.74	1.25	2.24	82.80	3.41	3.41	1.63	2.67	3.08
S2	715.69	1.65	3.62	75.75	2.14	2.14	1.25	2.48	2.55
S3	750.42	2.07	4.09	76.44	1.43	1.43	1.14	2.57	2.21
S4	1100.50	2.45	0.81	66.36	2.84	2.84	1.85	2.68	3.39
S5	1770.90	2.65	1.86	74.29	2.79	2.79	1.44	2.61	4.15
S6	1738.56	2.75	5.56	89.91	7.78	7.78	3.65	2.40	8.42
S7	1804.60	3.09	1.71	83.15	4.23	4.23	1.96	2.56	5.56
S8	300.00	3.61	3.20	81.31	4.51	4.51	2.46	2.48	6.72
S9	320.00	3.90	1.32	71.84	5.45	5.45	2.83	2.66	6.73

Notes: * Data is from Lu et al. (2023a). S_{non} is non-micropore specific surface area, V_{mic} is micropore volume, and V_{total} is the sum of micropore and non-micropore volume.

$$S_w = \frac{W/\rho_w}{Por/\rho_{apparent}} \tag{1}$$

where, W is water content, w. t.%; ρ_w is the density of water; S_w is water saturation; Por is porosity, %; $\rho_{apparent}$ is the apparent density of shale.

The MAC of a sample obtained from the adsorption experiment is the excess adsorption amount, and its absolute MAC can be converted by the Gibbs model:

$$n_e = n_a \cdot \left(1 - \frac{\rho_g}{\rho_{ad}}\right) \tag{2}$$

where, n_e and n_a are excess and absolute MAC, respectively, cm^3/g; ρ_g and ρ_{ad} are bulk phase and adsorbed phase densities, respectively, g/cm^3.

The adsorption experiment data was fitted using the Ono-Kondo model, which has been detailed in the references (Zhou et al., 2017a; Hu and Mischo, 2020), and its equation is given in Eq. (3).

$$n_e = \frac{n_0\rho_g(1 - e^{\frac{\varepsilon_s}{k\cdot T}})}{\frac{\rho_g\rho_{ad}}{\rho_{ad}-\rho_g} + \rho_{ad}e^{\frac{\varepsilon_s}{k\cdot T}}} \tag{3}$$

where, n_0 is the maximum MAC, cm^3/g; ε is the potential energy (J) associated with the interaction between CH_4 and adsorbent. k is the Boltzmann constant, and T is the absolute temperature.

2.3. Thermodynamics of adsorption

Adsorption thermodynamics can be used to determine the type of adsorption and indirectly reflect the adsorption force of the adsorbent on the adsorbate. The thermodynamic parameters include adsorption enthalpy (ΔH) and molar adsorption entropy (ΔS^0), which are used to describe the pressure-temperature relationship at an absolute adsorption constant. This relationship (Eq. (4)) can be derived from Tian et al. (2016).

$$\ln\left(\frac{P}{P_0}\right)_n = \frac{\Delta H}{RT} - \frac{\Delta S^0}{R} \tag{4}$$

where, ΔH is the adsorption enthalpy (kJ/mol), whose magnitude is equal to the equivalent adsorption heat (Q_{st}, $\Delta H = -Q_{st}$); ΔS^0 is the standard entropy of adsorption ($J\cdot mol^{-1}\ K^{-1}$); $P_0 = 0.1$ MPa; R is the ideal gas constant and T is the temperature (K).

2.4. GSC estimation under geological conditions

Due to the extremely low gas solubility of methane in water, the total gas basically includes only adsorbed gas and free gas. According to Pan et al. (2016), the GSC model under geological conditions can be expressed by Eq. (5–7). It should be pointed out that this model describes the maximum reservoir capacity under limited geological conditions.

$$n^H_{total} = n^H_e + \frac{Por\cdot(1 - S_w)}{\rho_{apparent}} \cdot \frac{\rho^H_g}{\rho^{STP}_g} \tag{5}$$

$$n^H_a = \frac{n^H_e \cdot \rho^H_a}{\rho^H_a - \rho^H_g} \tag{6}$$

$$n^H_{free} = n^H_{total} - n^H_a \tag{7}$$

where, n^H_{total}, n^H_a and n^H_{free} are the total storage capacity, adsorbed gas capacity and free gas capacity at H depth, cm^3/g, respectively; ρ^H_a, ρ^H_g and ρ^{STP}_g are the adsorbed phase density, free phase density and density at standard conditions at H depth, g/cm^3, respectively. Free phase density is from the NIST (national institute of standards and technology) database (Lemmon et al., 2022). n^H_e and ρ^H_a are calculated based on variable-temperature adsorption experiment data.

3. Results

3.1. Adsorption isotherms and data fitting

The HPMA results of MCT shale samples at 313.15 K and the adsorption isotherm curves fitted by the Ono-kondo model are shown in Fig. 1a. The model has a perfect fit to the measured data, with the fitting coefficient (R^2) of >0.99 (Table 1). The excess adsorption amount first increases rapidly with increasing pressure, reaching a maximum at about 8 MPa (0.83–2.99 cm^3/g), and then starts to decrease with a further increase of pressure. The absolute adsorption curves are shown in Fig. 1b. They rise with increasing pressure. The fitted parameters of the Ono-kondo model are summarized in Table 2. The maximum MAC of the nine samples is between 1.62 cm^3/g and 4.06 cm^3/g, with an average of 2.35 cm^3/g. ε_s/k ranges from −708.69 to −1179.35 K, with an average of −917.72 K. ρ_{ad} varies from 0.21 to 0.37 g/cm^3, with an average of 0.26 g/cm^3.

The shapes of the excess adsorption isotherms of the sample S7 at different temperatures and water saturation conditions are very similar (Fig. 2). Under dry conditions, the maximum n_e decreases from 1.57 cm^3/g to 0.98 cm^3/g as the temperature increases from 303.15 K to 363.15 K (Table 3 and Fig. 3a). Accordingly, n_0 reduces from 2.36 cm^3/g to 1.55 cm^3/g ε_s/k distributes between −992.34 K and −957.96 K, with an average of −976.62 K. ε_s is the potential energy of CH_4 molecules interacting with the shale pore surface. It is related to the surface properties and temperature (Sudibandriyo et al., 2010).

Under the moist conditions of the sample S7, as the S_w increases from 0 to 53.96%, the n_0 and maximum n_e all decrease significantly,

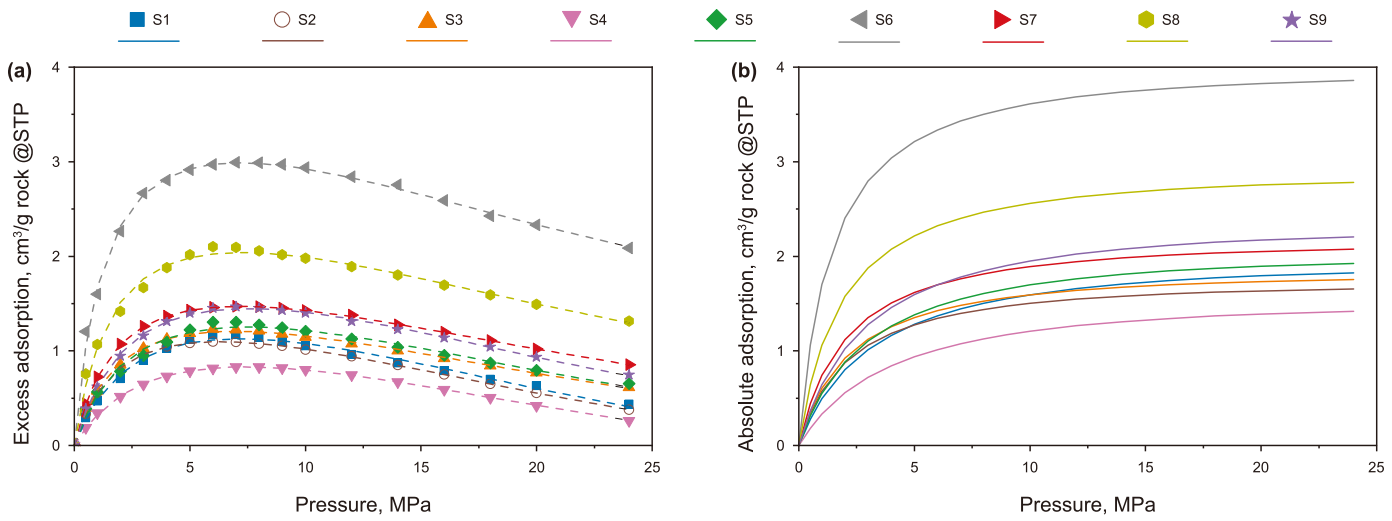

Fig. 1. Methane excess adsorption data and their fitted curves (a) and methane absolute adsorption curves from the Ono-Kondo model (b) for the MCT shale samples at 313.15 K.

Table 2
Fitting parameters from Ono-Kondo model (313.15 K).

Samples	n^{a}_{emax}, cm³/g	P^{b}_{nemax}, MPa	n^{c}_{0}, cm³/g	ε_s/k, K	ρ_{ad}, g/cm³	R^2	MAE[d]
S1	1.17	6	2.04	−779.98	0.216	0.99	0.025
S2	1.10	6	1.78	−896.68	0.217	0.99	0.001
S3	1.02	6	1.89	−943.66	0.255	0.99	0.014
S4	0.83	8	1.62	−708.69	0.206	0.99	0.004
S5	1.30	7	2.13	−845.24	0.247	0.99	0.033
S6	2.99	7	4.06	−1179.35	0.368	0.99	0.026
S7	1.47	6	2.23	−983.05	0.285	0.99	0.002
S8	2.10	6	2.97	−1056.71	0.314	0.99	0.036
S9	1.47	7	2.44	−856.84	0.251	0.99	0.013

Note: a: maximum excess MAC; b: pressure corresponding to n_{emax}. c: maximum MAC. d: mean absolute error.

from 2.23 cm³/g to 0.99 cm³/g and from 1.47 cm³/g to 0.60 cm³/g, respectively (Table 3 and Fig. 3b). This is due to the occupation of adsorption sites in the pores by water and the formation of water clusters through hydrogen bonding to block the pores (Gasparik et al., 2012).

3.2. Adsorbed phase density and adsorption space

Methane adsorption phase density is one of the basic parameters of the isothermal adsorption model of shales and can be obtained by fitting experimental data. It is strongly influenced by the temperature and adsorbent-adsorbate interaction. The liquid density is usually considered as the maximum adsorption phase density, and the critical density is the minimum (Do and Do, 2003; Rexer et al., 2013). As seen from the adsorbed phase densities (ρ_{ad}) of the studied samples derived from the ono-kondo model in Tables 2 and 3, they are reasonable, between the critical density and the boiling point liquid density (Fig. 4), without abnormally high values reported (Gasparik et al., 2012; Tian et al., 2016). At the same temperature conditions, ρ_{ad} shows a positive correlation with TOC contents (Fig. 4a). For the relevant results of the variable-temperature experiment of S7, ρ_{ad} decreases with increasing temperature, and they show a negative linear correlation (Fig. 4b).

Except for the sample S6 (high TOC), the adsorbed phase volume (V_{ad}) calculated from the maximum absolute MAC and ρ_a of other samples is slightly larger than the micropore pore volume (V_{mic}) (Fig. 5). At the same time, the diameter of CO_2 molecules is smaller than that of CH_4, hence the accessible space of V_{mic} obtained from the analysis of low-pressure CO_2 adsorption experiment should also be larger than the actual methane adsorption space in micropores. This indicates the existence of micropore filling and non-micropore surface adsorption of methane in shale pores, where the V_{ad} can only take up a portion of the total pore volume and most of the unexploited space in larger pores is filled with free methane, which is consistent with the results of Zhou et al. (2018) for the Longmaxi shale and Wei et al. (2021) for the Shuijingtuo shale.

3.3. Adsorption thermodynamic parameters

Based on Eq. (4), the thermodynamic parameters of S7 were calculated for the selected four different absolute methane adsorption amounts. As shown in Fig. 6a and Table 4, Q_{st} ranges from 17.66–24.38 (mean 20.98) kJ/mol. Since the adsorption heat of chemisorption is 40–600 kJ/mol (Chen et al., 2019), this adsorption on shale is physical sorption. ΔS^0 reflects the activity of the adsorbent and the behavioral characteristics of the adsorbent-adsorbate interaction (Xia et al., 2008). ΔS^0 for S7 ranges from −76.85 to −104.43 (mean −90.93) $J \cdot mol^{-1} K^{-1}$. The MCT shale in this study has a cast point in Fig. 6b between type III kerogen and clays, with a slightly larger Q_{st} and smaller ΔS^0 compared to the marine shale reported in the literature (Gasparik et al., 2014; Rexer et al., 2014; Chen et al., 2019; Hu and Mischo, 2020), showing a comparable methane adsorption performance with them.

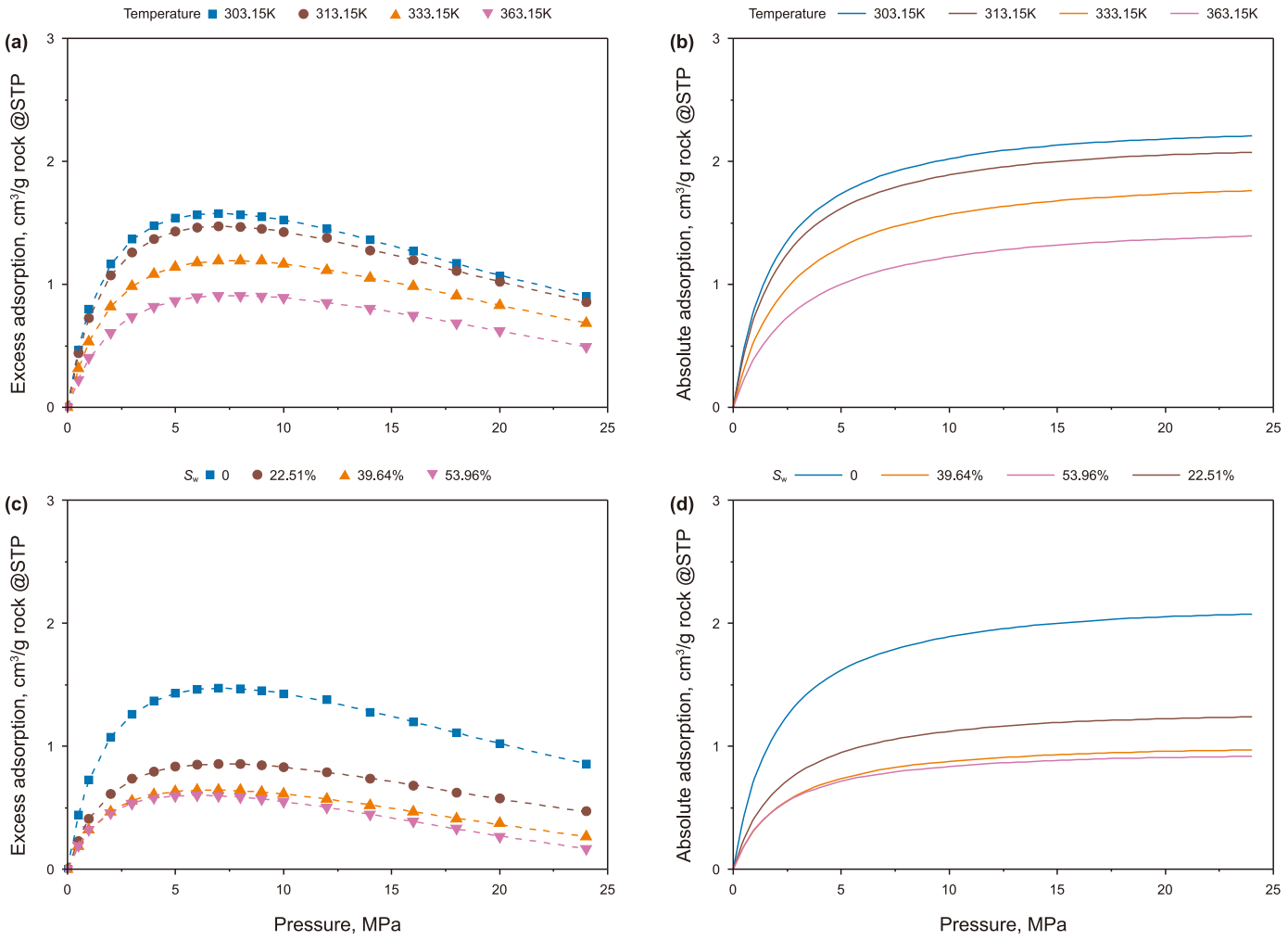

Fig. 2. Methane excess adsorption data and their fitted curves (a) and absolute adsorption curves (b) of the sample S7 at different temperatures (303.15 K, 313.15 K, 333.15 K, and 363.15 K). Methane excess adsorption data and their fitted curves (c) and absolute adsorption curves (d) of the sample S7 at different water saturation (0, 22.51%, 39.64% and 53.96%) at 313.15 K.

Table 3
Absorption parameters of S7 from the Ono-Kondo model at different temperature and water saturation conditions (the parameters are the same as those shown in Table 1).

Temperature, K	Saturation, %	n_{emax}, cm^3/g	P_{nemax}, MPa	n_0, cm^3/g	ϵ_s/k, K	ρ_{ad}, g/cm^3	R^2	MAE[d]
303.15	0	1.57	7	2.36	−992.34	0.300	0.99	0.003
313.15	0	1.47	6	2.23	−983.05	0.285	0.99	0.002
333.15	0	1.22	7	2.00	−973.11	0.248	0.99	0.001
363.15	0	0.98	7	1.55	−957.96	0.206	0.99	0.002
313.15	22.51	0.86	7	1.34	−946.33	0.269	0.99	0.003
313.15	39.64	0.64	7	1.05	−895.14	0.231	0.99	0.003
313.15	53.96	0.60	6	0.99	−888.81	0.204	0.99	0.002

4. Discussion

4.1. Influencing factors of maximum methane adsorption capacity

The maximum MAC of a shale is influenced by its TOC and clay mineral contents, organic matter type, maturity, pore structure, temperature and pressure. Among them, temperature and pressure can be simulated by setting experimental conditions, while these shale characteristic parameters affect each other. The TOC content primarily affects methane adsorption, which is the consensus of several studies (Gasparik et al., 2014). As shown in Fig. 7a, the maximum MAC of the samples in this study is also positively correlated with TOC content (r = 0.63). Maturity affects the development of OM pores (Chen and Xiao, 2014; Lu et al., 2023a), then affects sorption, with enhanced methane adsorption for samples with a similar TOC content as maturity increases. Compared with marine shales, the maximum MAC of the MCT samples is slightly lower under the conditions of the same TOC content and a comparable maturity. The methane adsorption capacity normalized to TOC for the studied samples across their maturity range also shows a positive synergistic relationship with R_o (Fig. 7b). In organic-rich shales, the contribution of clays to the shale MAC is small (Gasparik et al., 2014; Yang et al., 2015), which is because the adsorption of clay minerals is insignificant compared to

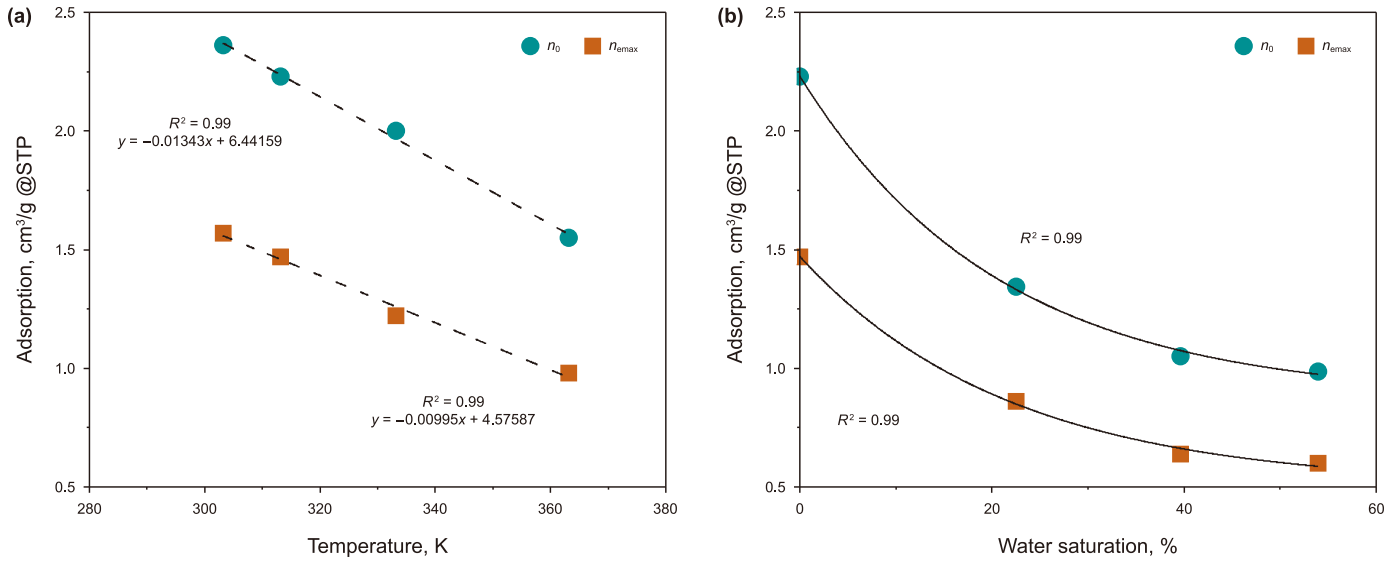

Fig. 3. Intersection plots of MAC with temperature (a) and water saturation (b).

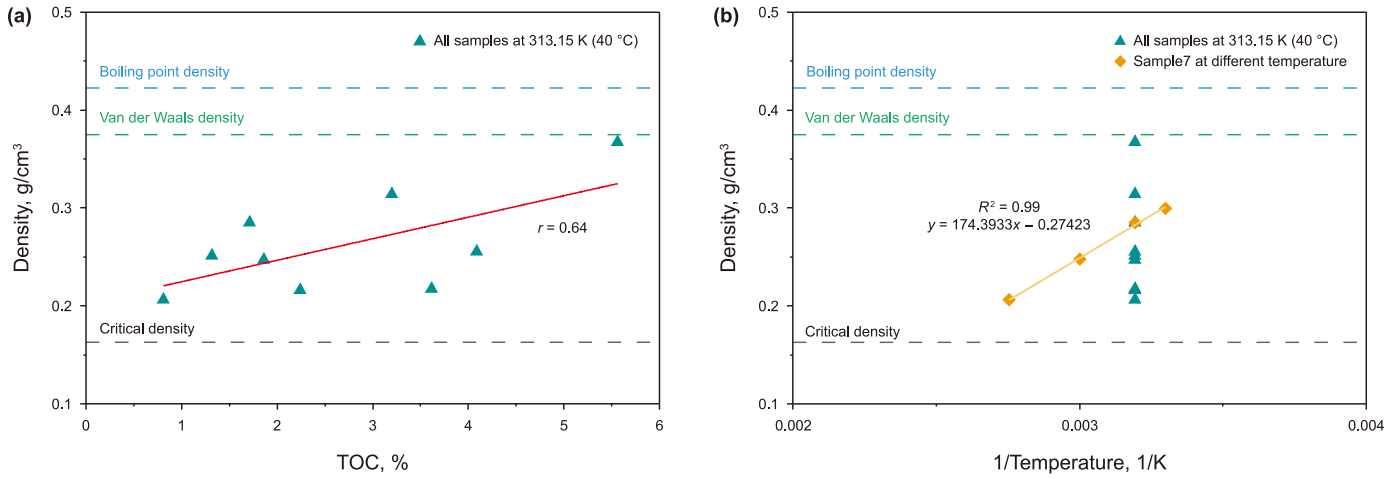

Fig. 4. Relationships of ρ_{ad} with TOC content at 313.15 K (a) and temperature (b). The comparison is made between fitted ρ_{ad} and approximate phase density.

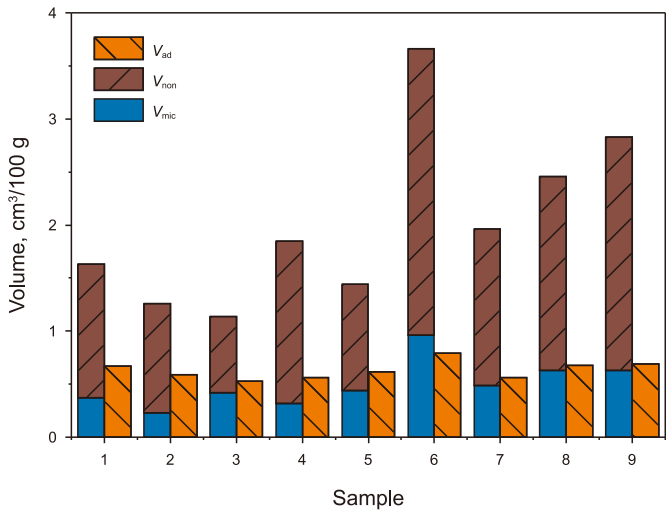

Fig. 5. Comparison of the V_{ad} and V_{mic}, and non-micropore volume (V_{non}) of the MCT shale samples.

that of kerogens (Ji et al., 2012; Zhang et al., 2012) (Fig. 7a). Although the total clays and the MAC in the studied samples show a certain degree of positive correlation (Fig. 7c), this is mainly due to the covariance between TOC and total clays in the MCT shale (Lu et al., 2023a). Therefore, this correlation is only a numerical, and not a causal one.

As shown in Fig. 7a, for samples with a similar TOC content, the higher the maturity, the greater the maximum MAC. Even for the same composition and maturity, the pore structure of different samples is also obviously variable. Furthermore, the TOC content covers different macerals, and the results of previous studies (Yang et al., 2019; Petersen et al., 2020) showed that the contribution of different macerals in adsorption varies greatly. Therefore, the prediction of maximum MAC from the shale composition is limited to specific shales with similar geochemical properties, and lacks generalizability.

In order to develop the MAC prediction model for the MCT shale of this study, the main factors affecting the shale adsorption performance need to be further discussed. These factors can be classified into two major categories. One is the shale property parameters, including TOC, clays, OM type and maturity, and

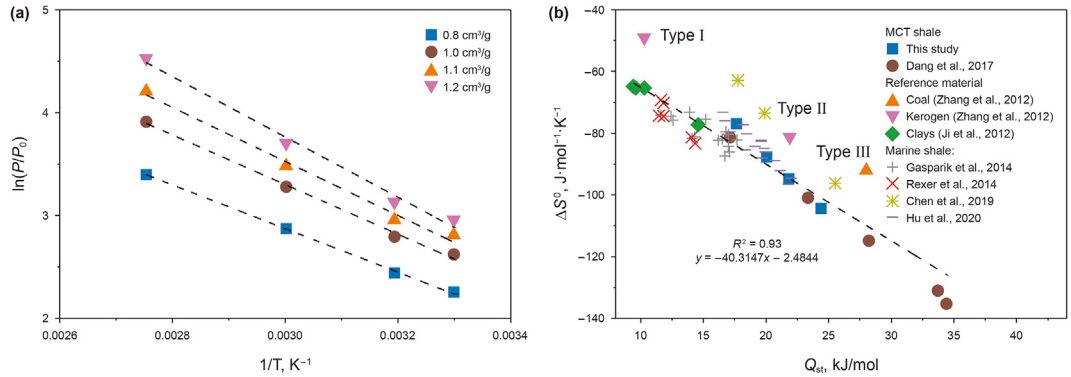

Fig. 6. (a) Thermodynamics of S7 under different MAC (STP). (b) The linear relationship between the Q_{st} and ΔS^0.

Table 4
Thermodynamic parameters of sample S7.

Absolute adsorption (cm^3/g, STP)	Q_{st} (kJ/mol)	ΔS^0 ($J \cdot mol^{-1}\ K^{-1}$)	Fitting line	R^2
0.8	17.66	−76.85	$y = -2123.42x + 9.24$	0.99
1.0	20.06	−87.64	$y = -2413.18x + 10.54$	0.99
1.1	21.83	−94.80	$y = -2625.40x + 11.40$	0.99
1.2	24.38	−104.43	$y = -2932.13x + 12.56$	0.99

another is the shale pore properties, i.e., nanopore structure parameters. In case the methane adsorption of shales assumes micropore volume filling and non-micropore surface adsorption (Do and Do, 2003; Zhou et al., 2017b; Sun et al., 2022), V_{mic} and S_{non} were chosen as the parameters of nanopore structure expression. The grey relational analysis (GRA) method as suggested by Azzeh et al. (2010) was used to analyze the influence degree of each factor on the MAC. Since all the samples in this study are type III kerogen, the subsequences of GRA are TOC content, clays content, maturity, V_{mic} and S_{non}, and MAC is the parent sequence. As shown in the ranking results (Table 5), the two pore structure parameters of the shale are more critical to MAC than its compositional properties. Thus, V_{mic} and S_{non} were used to build a multiple regression model of MAC (Eq. (8)). The evaluation results are shown in Table 6. The low values of mean absolute error, mean square error and root mean square error implicate a high accuracy of MAC prediction results.

$$MAC = 4.36335 \times V_{mic} + 0.01845 \times S_{non}, R^2 = 0.98 \quad (8)$$

4.2. Geological model of methane storage capacity

In order to build a geological model for predicting the methane content of MCT shales in the Qinshui Basin, the effects arising from the actual geological conditions should be considered. For this basin, using depth as the independent variable for the variety of geological conditions, the dependent variables mainly include the variation of temperature and pressure with depth and the variation of pore structure due to the variation of maturity with depth. The effects of temperature and pressure on shale adsorbed and free gas capacities can be linked through HPMA and free phase density, respectively (by Eq. (5–7)). Furthermore, the depth constraint on the pore structure can be achieved using the relationship between the depth and maturity in this study area.

The Qinshui Basin was formed in the middle Jurassic, and the Yanshanian tectonic thermal event from the late Jurassic to the end of the Cretaceous caused a substantial increase in the maturity of the Carboniferous-Permian MCT shales and massive methane generation (Su et al., 2005), but there is variability in different areas. In the southern part of the basin, there is a magmatic intrusion, leading to an unusual distribution of maturity (Li et al., 2006), while in the central and eastern part of the basin, along the Yushe-Wuxiang, the distribution of maturity and current depth show synergistic changes (Fig. 8a). Based on the data on the maturity and depth of MCT shales in this region (Yin and Guo, 2019; Zhang et al., 2019), a correlation plot of R_o versus depth is constructed (Fig. 8b, $r = 0.89$).

The results of Lu et al. (2023a) were used to correlate the pore structure of OM with R_o for the MCT shale in the Qinshui Basin. The evolution of porosity with the effect of buried stress was modeled using data derived from Miao et al. (2022) (Appendix for detailed calculations). Further, it was assumed that the composition and apparent density of the shale were constant, the pressure coefficient was 1, and the water saturation was 30%. Combining the above settings with the variable-temperature methane adsorption parameters under the dry conditions and the porosity and nanopore structure parameters of S7, the GSC based on the evolution of pore space (porosity and pore structure) with depth was calculated according to Eq. (5)–8, and the corresponding geological GSC model was established (subsequently referred to as the evolutive pore model) (Fig. 9). This model also compares the GSC model for this shale at the fixed porosity and pore structure parameters (subsequently referred to as constant pore model) conditions. For the evolutive pore model, the MAC increases rapidly with increasing depth, reaching a maximum at around 800 m, and then decreases slowly; the free gas and total gas capacities arise with increasing depth and go down slightly after >2800 m. The adsorbed gas capacity dominates at depths <1750 m, while the free gas capacity dominates at depths >1750 m. This shows some differences with the constant pore model. The GSC of the two models is essentially the same at about 1800 m. This is because this depth is essentially the actual depth of the study sample (S7), and both models have the same porosity and pore structure. However, at depth <1800 m, the total GSC based on the evolutive pore model is lower than that of the constant pore model, while at depth >1800 m, the former is greater than the latter, which is because the developed OM pores in

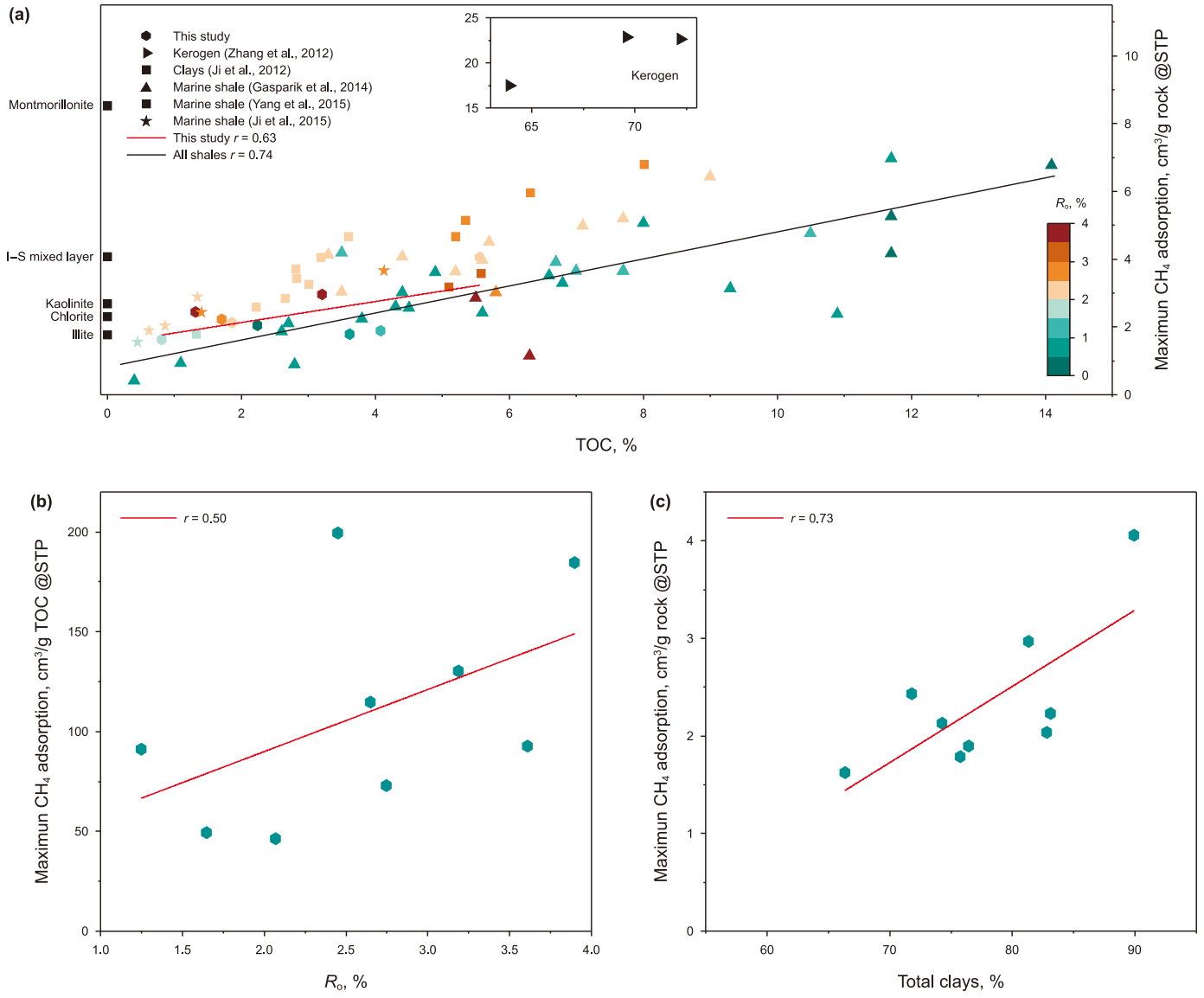

Fig. 7. (a) Plot of maximum MAC vs. TOC content of different shale samples. The color mapping represents maturity, and for the marine shales without vitrinite reflectance, their equivalent vitrinite reflectance is used. (b) Plot of R_o vs. TOC-normalized maximum CH_4 absolute adsorption of the studied MCT shales. (c) Plot of maximum MAC vs. total clays of the studied MCT shales.

Table 5
Grey relational degree of MAC.

Influencing factor		Degree	Rank
Pore structure parameters	V_{mic}	0.803	1
	S_{non}	0.680	2
Material characteristic parameters	Clays content	0.671	3
	R_o	0.628	4
	TOC content	0.553	5

Notes: Dimensionless processing mode: mean; Resolution coefficient $\rho = 0.5$.

Table 6
Evaluation of MAC prediction results.

Models	Mean absolute error	Mean square error	Root mean square error
Eq. (8)	0.2492	0.1104	0.3322

the shale at higher maturity stage increase the GSC. It is worth mentioning that for the constant pore model, the free gas capacity presents a continuous increase with the depth. At depth >2800 m, the total gas and free gas capacities of the evolutive pore model tend to decrease, which is a compound effect of the destruction of the OM pore structure at the over-maturity stage (Lu et al., 2023a)

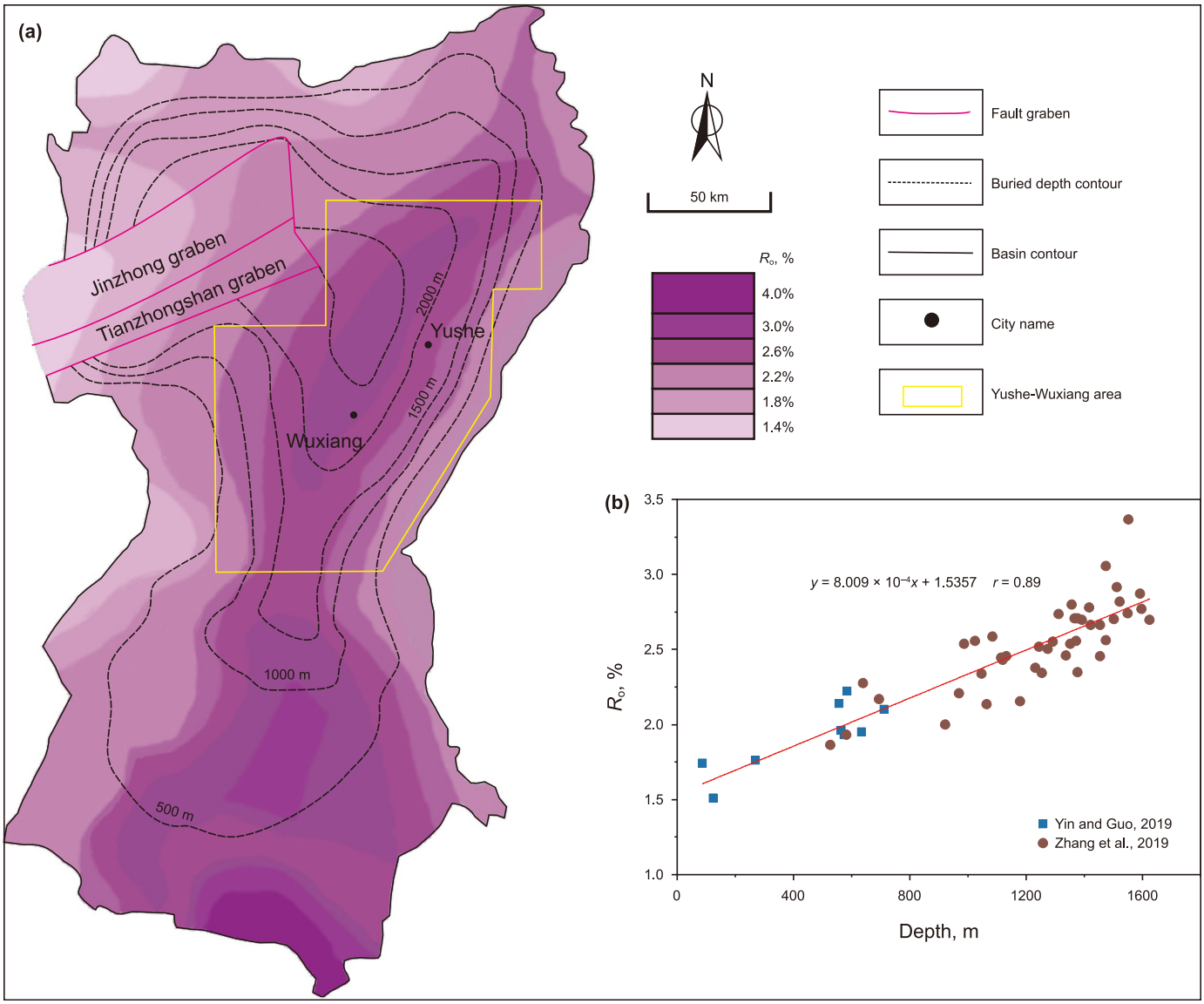

Fig. 8. (a) Planar distribution of maturity and current depth of Taiyuan-Shanxi formations in the Qinshui Basin. The R_o data come from Hou (2020). The depth is based on the data of the Carboniferous No.15 coal seam from Liu et al. (2022a,b). (b) Relationship between current depth and R_o in the Yushe-Wuxiang area.

and the compression of increased in-situ stress. It can be foreseen that the total GSC of the two models will intersect again at a certain depth (>2800 m), i.e., the total gas capacity of the evolutive pore model will be smaller than that of the constant pore model. However, this exceeds the maximum depth of the MCT shale in this area.

Reservoir pressure has an important influence on GSC and shale gas production. The commercially developed marine shale gas reservoirs in southern China have large burial depths, with a main pressure coefficient range of 0.9–2.0 (Jiang et al., 2023), while the MCT shale reservoirs in the Qinshui Basin have a shallower burial depth and a lower pressure coefficient. The pressure coefficient of coal reservoirs adjacent to the MCT shale in the Carboniferous-Permian strata is usually between 0.6 and 1.0 (Wang et al., 2017). The results of GSC calculated as pressure coefficients of 0.6, 0.7, 0.8, 0.9 and 1.0 respectively are shown in Fig. 10. The free gas capacity responds most significantly to pressure changes. It decreases rapidly with the decrease of the pressure coefficient, leading to a decline in the total GSC and an increase in the proportion of adsorbed gas. The adsorbed gas capacity is only affected by the pressure coefficient at the shallow depth (<1000 m), and as the depth >1000 m, the loss in adsorbed gas capacity is not significant as the pressure coefficient goes down.

4.3. Impact of water on adsorption gas and geological model of gas capacity

The water saturation of MCT shales in the Qinshui Basin ranges from about 25.5% to 76.4% (Sun et al., 2022). The presence of water in the shale pores affects the methane adsorption behavior and free gas space. Although the occupation of free gas storage space by water has been allowed in Eq. (5), the effects of water adsorption sites and the change in the interaction between adsorbent and sorbent, which affects methane adsorption, also need to be considered (Chalmers and Bustin, 2008). According to the study of Gasparik et al. (2012), with increasing water content in shales, the MAC will reduce until reaching a critical water saturation at which a further increase in water content has little effect on the MAC.

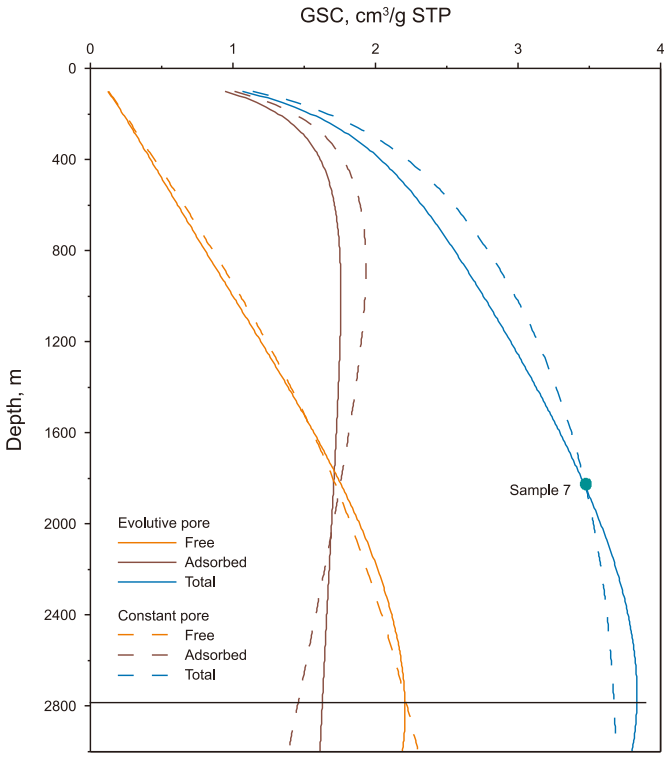

Fig. 9. Geological GSC models. A comparison is made between the evolutive pore model and the constant pore model. The two models are based on S7 (TOC = 1.71%, R_o = 3.09%, porosity = 5.56%) under the conditions of a pressure gradient of 1 MPa/100 m and a water saturation of 30%. The geothermal gradient and surface temperature of the Qinshui Basin are 28.2 K/km and 282.15 K, respectively, which come from Sun et al. (2006).

Based on this rule, combined with previous experimental data at different water contents (Table 7), an asymptotic model ($y = a + b \times c^x$) can be used to describe the MAC of the sample in the present study with increasing water saturation (Fig. 11).

As shown in Table 7, the asymptotic model well fits the data of the MCT shale sample of this study and marine shales. In the fitted equation, the value of $(a + b)$ is close to the MAC of dry samples, a is the MAC after reaching the critical water saturation, b is the maximum loss of adsorption due to the presence of water, and then $b/(a + b)$ is the maximum percentage of MAC loss due to water. The value of c can reflect the decreasing MAC of shale with increasing water saturation. Overall, water has a greater influence on the adsorption of the MCT shale sample (S7) than that of the marine shales, with the maximum percentage of MAC loss as high as 60.82%.

According to the S_w data of MCT shale in the Qinshui Basin (Sun et al., 2022), the range of water saturation is set from 20% to 70%. According to the evolutive pore model (section 4.2), the GSC model of S7 under different water saturation conditions was further constructed based on the asymptotic model of the effect of water on adsorption (Fig. 12). As the S_w increases from 20% to 70%, the free and total gas capacities decline significantly, and the adsorbed gas capacity does not decrease significantly after S_w > 50%. Compared with the model under dry conditions (Fig. 9), the total GSC decreases from 31.30% to 4.64% under water conditions (from 500 m to 2800 m, respectively, Fig. 12c), i.e., the difference between the two models decreases with increasing depth. This is because the reduction of the adsorption gas allows the conversion of the adsorption phase volume into the storage space for the free gas. For the same water saturation of 30%, the free gas capacity of this model is significantly greater than that of the model based on the absorption parameters under dry conditions (Fig. 12a).

The total gas of 2 m^3/t is used as the baseline of the marine shale gas reservoirs with commercial potential in China (Wang et al., 2012). If this standard is adopted for the MTC shale of the present study, the depth corresponding to this gas content increases significantly with rising water saturation according to the prediction results of Fig. 12c. For instance, the shale reaches a total GSC of 2 m^3/t at the depth of 680 m and 1520 m as the water saturation is 20% and 50%, respectively. When the water saturation exceeds 60%, even if the depth reaches 2800 m (the greatest depth in the study area), the GSC of the shale does not reach 2 m^3/t, i.e., without economic development potential (Fig. 12c). For this lower TOC content MCT shale, the shale gas exploration should be directed to deeper depths (>1000–1500 m), especially to blocks with lower water saturation.

4.4. Uncertainties and limitations of the GSC model

In the geological GSC model of Fig. 12, the effect of S_w on adsorption is based on the shale with equilibrium water. During the equilibrium water experiments, the water molecules enter the shale nanopores from the outside to the inside, while the transport of shale connate water is from the inside to the outside. This means that the equilibrium water and connate water would have different distributions in the shale nanopore system, which may affect the adsorption. In addition to this, the models describing the effect of water on MAC have not been implemented for different temperature conditions. The main reason is related to two uncertainties in the HPMA experiments of water-bearing shales. One is that water molecules will separate from the sample during the evacuation, and another is that if different temperature gradients are set in the experiments, higher temperature conditions will cause a significant loss of water molecules from the shale, thus affecting the experimental results. Most of the MAC data for water-bearing shales reported in the literature (Shabani et al., 2018; Ren et al., 2019) are based on low-temperature experiments (e.g., ≤318.15 K). These also corroborate the difficulty of maintaining the water content in shales in high-temperature experiments.

In this study, the relationship between maturity and depth of MCT shale is limited to the Yushe-Wuxiang area to ensure their high correlation coefficient. The effect of maturity not only affects the pore structure of OM but also changes its molecular structure, i.e., as maturity increases, the aromatization of OM molecular structure would be more favorable for methane adsorption (Zhang et al., 2012). However, it has also been shown that differences in surface functional groups have negligible effects on MAC in high and over-mature shales, and that their pore structure mainly influences adsorption (Li et al., 2022), with basically physisorbed mechanism (Fig. 6b). Nevertheless, the effect of the chemical structure evolution of OM on methane adsorption also deserves further study and consideration.

The GSC model constructed with the S7 sample represents the MCT shale with a lower TOC content, which can characterize most of the shale strata in the Qinshui Basin. However, there are also a few shales with a higher TOC content in this basin whose GSC characteristics and models need further investigation. It should be also noted that the GSC model proposed in this study represents the capacity for gas storage, i.e., it is assumed that there are sufficient gas sources in the shale reservoir. Under actual geological conditions, the GSC of shales may be influenced by more factors, such as their gas generation potential and the gas expulsion efficiency, therefore, the model needs to be further validated by obtaining shale gas exploration and development data.

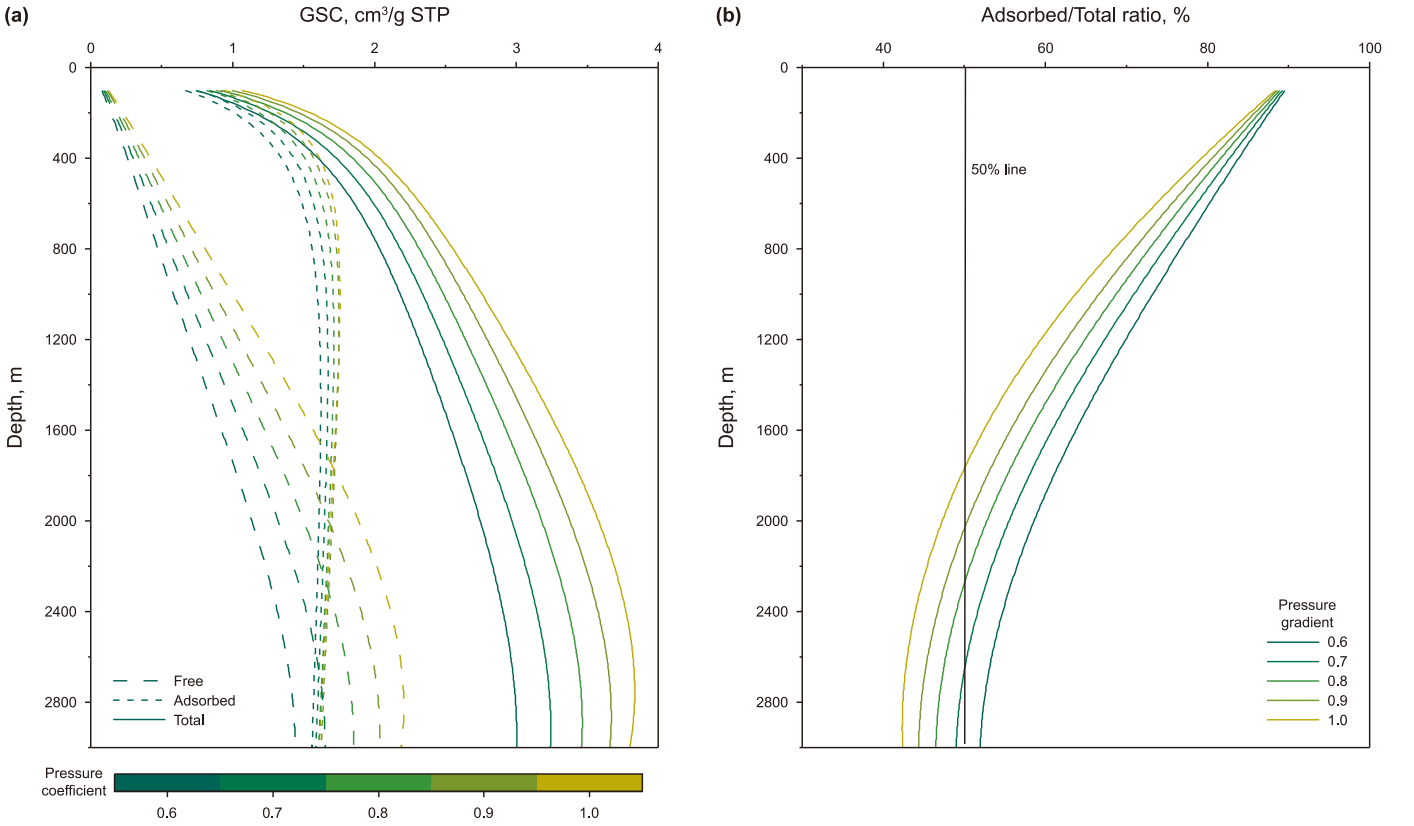

Fig. 10. Variation of GSC with depth (a) and adsorbed gas/total gas ratio as a function of depth (b) under different pressure coefficients.

Table 7
The parameters of asymptotic models for different shales.

	Haynesville	CN_33	S3	S4	S7
MAC, cm^3/g	4.48	2.64	3	6.54	2.23
R_o, %	2.5	2.8	1.28	1.69	3.09
TOC, %	3.1	0.96	5.79	10.94	1.71
Clays, %	47.8	45.5	4	3	83.15
a	2.4517	1.1192	1.8681	4.9801	0.8741
b	2.0289	1.5429	1.1382	1.5601	1.357
c	0.9489	0.9416	0.9884	0.9712	0.9528
R^2	0.99	0.96	0.97	0.99	0.99
$a + b$	4.4806	2.6621	3.0063	6.5402	2.2311
$b/(a+b)$	45.28%	57.96%	37.86%	23.85%	60.82%
Data source	Marine shale (Merkel et al., 2015)	Marine shale (Yang et al., 2016)	Marine shale (Shabani et al., 2018)		MCT shale in this study

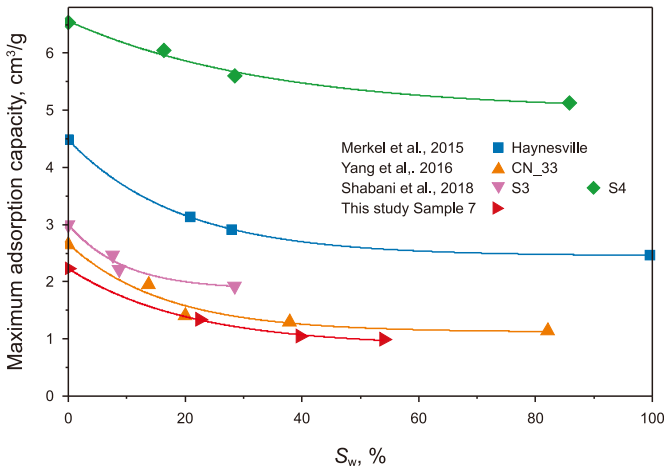

Fig. 11. MAC as a function of water saturation (S_w).

5. Conclusions

This work established an experimental and simulation combination method to explore the HPMA characteristics of MCT shale samples from the Qinshui Basin and the GSC considering the approximate geological conditions.

From the results, compared to the composition characteristics, the shale pore structure parameters of V_{mic} and S_{non} have priority in the effect on the methane adsorption. The methane adsorption prediction model based on the two pore structure parameters shows promising predictive performance.

There are differences between the GSC obtained from the evolutive pore model proposed in this study and the conventional constant pore model. The main reason is the evolution of pore structure governed by the depth of the shale.

For the lower TOC content MCT shales, depth, pressure coefficient and water saturation together constrain their shale gas potentials. Even considering the maximum possible pressure coefficient of 1.0, the GSC of the shale does not reach the low limit

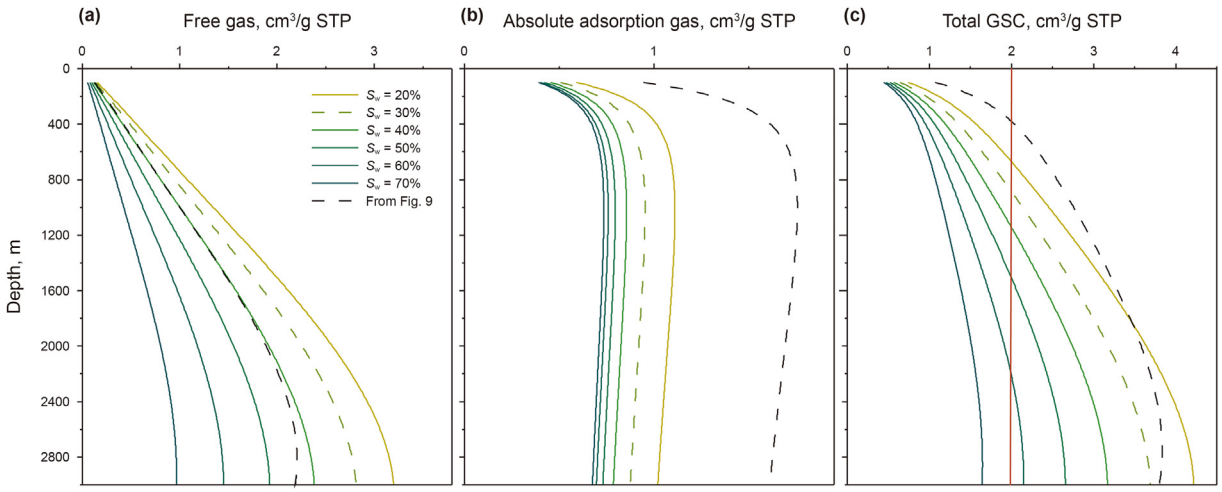

Fig. 12. GSC model considering the effect of water. Free gas (a), absolute adsorption gas (b) and total gas (c) capacities with water saturation from 20% to 70%. Pressure gradient = 1 MPa/100 m. The model in Fig. 9 is also shown in this figure for a comparison when S_w = 30%.

of development potential (2 m^3/t) when the depth is < 800 m / water saturation >60%. Therefore, the exploration and development of shale gas should be carried out in areas with greater depths, especially in areas with low water saturation.

CRediT authorship contribution statement

Chen-Gang Lu: Conceptualization, Writing – original draft, Data curation, Funding acquisition, Methodology, Resources, Software. **Xian-Ming Xiao:** Funding acquisition, Project administration, Supervision. **Zhen-Qian Xue:** Conceptualization, Writing – original draft. **Zhang-Xin Chen:** Supervision, Writing – review & editing. **Yin-Tao Dong:** Methodology, Software. **Yue Feng:** Data curation, Investigation. **Gang Li:** Resources.

Declaration of competing interest

The authors declare that they have no known competing financial interests or personal relationships that could have appeared to influence the work reported in this paper.

Acknowledgments

We would like to thank the reviewers and editor for their insightful comments and suggestions that significantly enhanced the quality of the manuscript. This work was jointly supported by the Science and Technology Department of Shanxi Province, China (20201101003), the National Natural Science Foundation of China (U1810201) and the China Scholarship Council (202206400012).

Appendix A. Supplementary data

Supplementary data to this article can be found online at https://doi.org/10.1016/j.petsci.2024.03.027.

References

Abdollahi, R., Motahhari, S., Askari, A., Hematpur, H., Zamani, Z., Tirtashi, R., Daryabandeh, M., Chen, H., 2022. A systematic step-wise approach for shale gas assessment in undeveloped prospects: a case study of Lurestan shale gas area in Iran. Petrol. Explor. Dev. 49 (3), 596–604. https://doi.org/10.1016/S1876-3804(22)60049-1.

Azzeh, M., Neagu, D., Cowling, P.I., 2010. Fuzzy grey relational analysis for software effort estimation. Empir. Software Eng. 15 (1), 60–90. https://doi.org/10.1007/s10664-009-9113-0.

Cander, H., 2012. Sweet Spots in Shale Gas and Liquids Plays: Prediction of Fluid Composition and Reservoir Pressure. AAPG Annual Convention and Exhibition.

Chalmers, G.R.L., Bustin, R.M., 2008. Lower Cretaceous gas shales in northeastern British Columbia; Part I, Geological controls on methane sorption capacity. Bull. Can. Petrol. Geol. 56 (1), 1–21. https://doi.org/10.2113/gscpgbull.56.1.1.

Chalmers, G.R.L., Bustin, R.M., Power, I.M., 2012. Characterization of gas shale pore systems by porosimetry, pycnometry, surface area, and field emission scanning electron microscopy/transmission electron microscopy image analyses: examples from the Barnett, Woodford, Haynesville, Marcellus, and Doig units. AAPG Bull. 96, 1099–1119. https://doi.org/10.1306/10171111052.

Chen, J., Xiao, X.M., 2014. Evolution of nanoporosity in organic-rich shales during thermal maturation. Fuel 129, 173–181. https://doi.org/10.1016/j.fuel.2014.03.058.

Chen, L., Zuo, L., Jiang, Z.X., Jiang, S., Liu, K.Y., Tan, J.Q., Zhang, L.C., 2019. Mechanisms of shale gas adsorption: evidence from thermodynamics and kinetics study of methane adsorption on shale. Chem. Eng. J. 361, 559–570. https://doi.org/10.1016/j.cej.2018.11.185.

Clarkson, C.R., Haghshenas, B., 2016. Characterization of multi-fractured horizontal shale wells using drill cuttings: 1. Fluid-in-place estimation. J. Nat. Gas Sci. Eng. 32, 574–585. https://doi.org/10.1016/j.jngse.2016.02.056.

Dang, W., Zhang, J.C., Wei, X.L., Tang, X., Chen, Q., Li, Z.M., Zhang, M.C., Liu, J., 2017. Geological controls on methane adsorption capacity of Lower Permian transitional black shales in the Southern North China Basin, Central China: experimental results and geological implications. J. Petrol. Sci. Eng. 152, 456–470. https://doi.org/10.1016/j.petrol.2017.03.017.

Do, D.D., Do, H.D., 2003. Adsorption of supercritical fluids in non-porous and porous carbons: analysis of adsorbed phase volume and density. Carbon 41 (9), 1777–1791. https://doi.org/10.1016/S0008-6223(03)00152-0.

Dong, D.Z., Qiu, Z., Zhang, L.F., Li, S.X., Zhang, Q., Li, X.T., Zhang, S.R., Liu, H.L., Wang, Y.M., 2021. Progress on sedimentology of transitional facies shales and new discoveries of shale gas. Act. Sed. Sin. 39 (1), 29–45. https://doi.org/10.14027/j.issn.1000-0550.2021.002 (in Chinese).

EIA, U.S.E.I., 2022. Proved Reserves of Crude Oil and Natural Gas in the United States. Washington.

Feng, Y., Xiao, X.M., Wang, E.Z., Gao, P., Lu, C.G., Li, G., 2023a. Gas storage in shale pore system: a review of the mechanism, control and assessment. Petrol. Sci. 20 (5), 2605–2636 j.petsci.2023.05.012.

Feng, Y., Xiao, X.M., Gao, P., Wang, E.Z., Hu, D.F., Liu, R.B., Li, G., Lu, C.G., 2023b. Restoration of sedimentary environment and geochemical features of deep marine Longmaxi shale and its significance for shale gas: a case study of the Dingshan area in the Sichuan Basin, South China. Mar. Petrol. Geol. 151, 106186. https://doi.org/10.1016/j.marpetgeo.2023.106186.

Gao, P., Xiao, X.M., Hu, D.F., Lash, G., Liu, R.B., Cai, Y.D., Wang, Z.H., Zhang, B.Y., Yuan, T., Liu, S.Y., 2022. Effect of silica diagenesis on porosity evolution of deep gas shale reservoir of the Lower Paleozoic Wufeng-Longmaxi formations, Sichuan Basin. Mar. Petrol. Geol. 145, 105873. https://doi.org/10.1016/j.marpetgeo.2022.105873.

Gasparik, M., Bertier, P., Gensterblum, Y., Ghanizadeh, A., Krooss, B., Littke, R., 2014. Geological controls on the methane storage capacity in organic-rich shales. Int. J. Coal Geol. 123, 34–51. https://doi.org/10.1016/j.coal.2013.06.010.

Gasparik, M., Ghanizadeh, A., Bertier, P., Gensterblum, Y., Bouw, S., Krooss, B., 2012. High-pressure methane sorption isotherms of black shales from The Netherlands. Energy Fuel. 26 (8), 4995–5004. https://doi.org/10.1021/ef300405g.

Guo, S.B., Wang, Z.L., Ma, X., 2021. Exploration prospect of shale gas with Permian transitional facies of some key areas in China. Pet. Geophys. Explor. 43 (3),

377–385+414. https://doi.org/10.11781/sysydz202103377 (in Chinese).
Hou, X.W., 2020. Study on Gas Controlling Mechanism and Coupled Accumulation of Deep Coal Measure Gases in Qinshui Basin. China university of Mining and technology, p. 273 (in Chinese).
Hu, K., Mischo, H., 2020. High-pressure methane adsorption and desorption in shales from the Sichuan basin, Southwestern China. Energy Fuel. 34 (3), 2945–2957. https://doi.org/10.1021/acs.energyfuels.9b04142.
Hu, K., Tang, J.R., Mischo, H., 2021. Investigation of supercritical shale gas adsorption in shale based on the Ono-Kondo lattice model. J. China Coal Soc. 46 (8), 2479–2487. https://doi.org/10.13225/j.cnki.jccs.CB21.0783 (in Chinese).
Ji, L.M., Zhang, T.W., Milliken, K.L., Qu, J.L., Zhang, X.L., 2012. Experimental investigation of main controls to methane adsorption in clay-rich rocks. Appl. Geochem. 27 (12), 2533–2545. https://doi.org/10.1016/j.apgeochem.2012.08.027.
Ji, W.M., Song, Y., Jiang, Z.X., Chen, L., Li, Z., Yang, X., Meng, M.M., 2015. Estimation of marine shale methane adsorption capacity based on experimental investigations of Lower Silurian Longmaxi formation in the Upper Yangtze Platform, south China. Mar. Petrol. Geol. 68, 94–106. https://doi.org/10.1016/j.marpetgeo.2015.08.012.
Jiang, P.F., Wu, J.F., Zhu, Y.Q., Zhang, D.K., Wu, W., Zhang, R., Wu, Z., Wang, Q., Yang, Y.R., Yang, X., Wu, Q.Z., Chen, L.Q., He, Y.F., Zhang, J., 2023. Enrichment conditions and favorable areas for exploration and development of marine shale gas in Sichuan Basin. Acta Pet. Sin. 44 (1), 91–109. https://doi.org/10.7623/syxb202301006 (in Chinese).
Jiang, W.B., Cao, G.H., Luo, C., Lin, M., Ji, L.L., Zhou, J., 2022. A composition-based model for methane adsorption of overmature shales in Wufeng and Longmaxi Formation, Sichuan Basin. Chem. Eng. J. 429, 130766. https://doi.org/10.1016/j.cej.2021.130766.
Jiang, Z., Zhao, L., Zhang, D.X., 2018. Study of adsorption behavior in shale reservoirs under high pressure. J. Nat. Gas Sci. Eng. 49, 275–285. https://doi.org/10.1016/j.jngse.2017.11.009.
Lemmon, E.W., Bell, I.H., Huber, M.L., McLinden, M.O., 2022. Thermophysical properties of fluid systems. In: NIST Chemistry WebBook, NIST Standard Reference Database Number 69. National Institute of Standards and Technology, Gaithersburg MD, 20899.
Li, T.F., Tian, H., Xiao, X.M., Cheng, P., Zhou, Q., Wei, Q., 2017. Geochemical characterization and methane adsorption capacity of overmature organic-rich Lower Cambrian shales in northeast Guizhou region, southwest. China. Mar. Petrol. Geol. 86, 858–873. https://doi.org/10.1016/j.marpetgeo.2017.06.043.
Li, W., Stevens, L.A., Zhang, B., Zheng, D.Y., Snape, C., 2022. Combining molecular simulation and experiment to prove micropore distribution controls methane adsorption in kerogens. Int. J. Coal Geol. 261, 104092. https://doi.org/10.1016/j.coal.2022.104092.
Li, W., Zhang, Z.H., Yang, Y.C., Han, L.G., Shao, M.H., 2006. Constraining the hydrocarbon expulsion history of the coals in Qinshui Basin, North China, from the analysis of fluid inclusions. J. Geochem. Explor. 89 (1–3), 222–226. https://doi.org/10.1016/j.gexplo.2005.11.047.
Liu, D.M., Jia, Q.F., Cai, Y.D., Gao, C.J., Qiu, F., Zhao, Z., Chen, S.Y., 2022a. A new insight into coalbed methane occurrence and accumulation in the Qinshui Basin, China. Gondwana Res. 111, 280–297. https://doi.org/10.1016/j.gr.2022.08.011.
Liu, X.Y., Zhang, L.H., Li, S.X., Zhang, J.H., Zhao, Y.L., Zhang, R.H., Guo, J.J., Tang, H.Y., Zhang, F., 2022b. Supercritical methane isothermal adsorption model considering multiple adsorption mechanisms in shale. Acta Pet. Sin. 43 (10), 1487–1499. https://doi.org/10.7623/syxb202210011 (in Chinese).
Lu, C.G., Xiao, X.M., Gai, H.F., Feng, Y., Li, G., Meng, G.M., Gao, P., 2023a. Nanopore structure characteristics and evolution of type III kerogen in marine-continental transitional shales from the Qinshui basin, northern China. Geoe. Sci. and Eng, 211413. https://doi.org/10.1016/j.geoen.2022.211413.
Lu, C.G., Xiao, X.M., Xue, Z.Q., Chen, Z.X., Li, G., Feng, Y., 2023b. Fractal and multifractal characteristics of nanopores and their controlling factors in marine–continental transitional shales and their kerogens from Qinshui Basin, northern China. Nat. Resour. Res. 32 (5), 2313–2336. https://doi.org/10.1007/s11053-023-10222-3.
Merkel, A., Fink, R., Littke, R., 2015. The role of pre-adsorbed water on methane sorption capacity of Bossier and Haynesville shales. Int. J. Coal Geol. 147–148, 1–8. https://doi.org/10.1016/j.coal.2015.06.003.
Miao, F., Wu, D., Liu, X.Y., Xiao, X.C., Zhai, W.B., Geng, Y.Y., 2022. Methane adsorption on shale under in situ conditions: gas-in-place estimation considering in situ stress. Fuel 308, 121991. https://doi.org/10.1016/j.fuel.2021.121991.
Okolo, G.N., Everson, R.C., Neomagus, H.W.J.P., Sakurovs, R., Grigore, M., Bunt, J.R., 2019. The carbon dioxide, methane and nitrogen high-pressure sorption properties of South African bituminous coals. Int. J. Coal Geol. 209, 40–53. https://doi.org/10.1016/j.coal.2019.05.003.
Pan, L., Xiao, X.M., Tian, H., Zhou, Q., Cheng, P., 2016. Geological models of gas in place of the Longmaxi shale in southeast Chongqing, south China. Mar. Petrol. Geol. 73, 433–444. https://doi.org/10.1016/j.marpetgeo.2016.03.018.
Petersen, H.I., Sanei, H., Gelin, F., Loustaunau, E., Despujols, V., 2020. Kerogen composition and maturity assessment of a solid bitumen-rich and vitrinite-lean shale: insights from the Upper Jurassic Vaca Muerta shale, Argentina. Int. J. Coal Geol. 229, 103575. https://doi.org/10.1016/j.coal.2020.103575.
Ren, W.X., Guo, J.C., Zeng, F.H., Wang, T.Y., 2019. Modeling of high-pressure methane adsorption on wet shales. Energy Fuel. 33 (8), 7043–7051.
Ren, W.X., Zhou, Y., Guo, J.C., Wang, T.Y., 2022. High-pressure adsorption model for middle-deep and deep shale gas. Earth Sci. 47 (5), 1865–1875. https://doi.org/10.1021/acs.energyfuels.9b01024 (in Chinese).
Rexer, T.F., Benham, M.J., Aplin, A.C., Thomas, K.M., 2013. Methane adsorption on shale under simulated geological temperature and pressure conditions. Energy Fuel. 27 (6), 3099–3109. https://doi.org/10.1021/ef400381v.
Rexer, T.F., Mathia, E.J., Aplin, A.C., Thomas, K.M., 2014. High-pressure methane adsorption and characterization of pores in Posidonia shales and isolated kerogens. Energy Fuel. 28 (5), 2886–2901. https://doi.org/10.1021/ef402466m.
Sakurovs, R., Day, S., Weir, S., Duffy, G., 2007. Application of a modified Dubinin-Radushkevich equation to adsorption of gases by coals under supercritical conditions. Energy Fuel. 21 (2), 992–997. https://doi.org/10.1021/ef0600614.
Shabani, M., Moallemi, S.A., Krooss, B.M., Alexandra, A.H., Ziba, Z.P., Ghalavand, H., Littke, R., 2018. Methane sorption and storage characteristics of organic-rich carbonaceous rocks, Lurestan province, southwest Iran. Int. J. Coal Geol. 186, 51–64. https://doi.org/10.1016/j.coal.2017.12.005.
Song, X., Lü, X.X., Shen, Y.Q., Guo, S., Guan, Y., 2018. A modified supercritical Dubinin–Radushkevich model for the accurate estimation of high pressure methane adsorption on shales. Int. J. Coal Geol. 193, 1–15. https://doi.org/10.1016/j.coal.2018.04.008.
Su, X.B., Lin, X.Y., Zhao, M.J., Song, Y., Liu, S.B., 2005. The upper Paleozoic coalbed methane system in the Qinshui basin, China. AAPG Bull. 89 (1), 81–100. https://doi.org/10.1306/07300403125.
Sudibandriyo, M., Mohammad, S.A., Robinson, R.L., Gasem, K.A.M., 2010. Ono–Kondo lattice model for high-pressure adsorption: pure gases. Fluid Phase Equil. 299 (2), 238–251. https://doi.org/10.1016/j.fluid.2010.09.032.
Sun, J., Xiao, X.M., Cheng, P., 2022. Methane absorption of coal-measure shales with and without pore water from the Qinshui Basin, North China: based on high-pressure methane absorption experiments. Int. J. Coal Geol. 263, 104116. https://doi.org/10.1016/j.coal.2022.104116.
Sun, Z.X., Zhang, W., Hu, B.Q., Pan, T.Y., 2006. Features of heat flow and the geothermal field of the Qinshui Basin. Chin. J. Geophys. 49 (1), 130–134 (in Chinese).
Tian, H., Li, T.F., Zhang, T.W., Xiao, X.M., 2016. Characterization of methane adsorption on overmature Lower Silurian–Upper Ordovician shales in Sichuan Basin, southwest China: experimental results and geological implications. Int. J. Coal Geol. 156, 36–49. https://doi.org/10.1016/j.coal.2016.01.013.
Wang, F.Y., Guan, J., Feng, W.P., Bao, L.Y., 2013. Evolution of overmature marine shale porosity and implication to the free gas volume. Petrol. Explor. Dev. 40 (6), 819–824. https://doi.org/10.1016/S1876-3804(13)60111-1.
Wang, J., Bao, H.Y., Lu, Y.Q., Liu, Y., Zhang, M.Y., 2019. Quantitative characterization and main controlling factors of shale gas occurrence in Jiaoshiba area, Fuling. Earth Sci. 44 (3), 1001–1011 (in Chinese).
Wang, M.Z., Wang, B., Sun, F.J., Zhao, Y., Cong, L.Z., Yang, J.S., Yu, R.Z., Luo, J.Y., Zhou, H.M., 2017. Quantitative evaluation of CBM enrichment and high yield of Qinshui Basin. Nat. Gas Geosci. 28 (7), 1108–1114. https://doi.org/10.11764/j.issn.1672-1926.2017.06.016 (in Chinese).
Wang, S.J., Yang, T., Zhang, G.S., Li, D.H., Chen, X.M., 2012. Shale gas enrichment factors and the selection and evaluation of the core area. Strategic Study of Cae 14 (6), 94–100. https://doi.org/10.3969/j.issn.1009-1742.2012.06.013 (in Chinese).
Wei, S.L., He, S., Hu, M.Y., Yang, W., Guo, X.W., Iglauer, S., Zhai, G.Y., 2021. Supercritical high-pressure methane adsorption on the lower Cambrian Shuijingtuo shale in the Huangling anticline area, south China: adsorption behavior, storage characteristics, and geological implications. Energy Fuel. 35 (24), 19973–19985. https://doi.org/10.1021/acs.energyfuels.1c02702.
Xia, X., Naumann D Alnoncourt, R., Muhler, M., 2008. Entropy of adsorption of carbon monoxide on energetically heterogeneous surfaces. J. Therm. Anal. Calorim. 91 (1), 167–172. https://doi.org/10.1007/s10973-007-8440-x.
Xiao, X.M., Wang, M.L., Wei, Q., Tian, H., Pan, L., Li, T.F., 2015. Evaluation of lower Paleozoic shale with shale gas prospect in south China. Nat. Gas Geosci. 26 (8), 1433–1445. https://doi.org/10.11764/j.issn.1672/1926.2015.08.1433 (in Chinese).
Xin, D., Tang, S.H., Zhang, S.H., Xi, Z.D., 2021. Declining high-pressure sorption isotherms on shale and coal: systematic comparison of the contributing factors. Energy Fuel. 35 (19), 15695–15708. https://doi.org/10.1021/acs.energyfuels.1c02455.
Yang, C., Xiong, Y.Q., Zhang, J.C., Liu, Y.K., Chen, C., 2019. Comprehensive understanding of OM-hosted pores in transitional shale: a case study of Permian Longtan shale in south China based on organic petrographic analysis, gas adsorption, and X-ray diffraction measurements. Energy Fuel. 33 (9), 8055–8064. https://doi.org/10.1021/acs.energyfuels.9b01410.
Yang, F., Ning, Z.F., Zhang, R., Zhao, H.W., Krooss, B.M., 2015. Investigations on the methane sorption capacity of marine shales from Sichuan Basin, China. Int. J. Coal Geol. 146, 104–117. https://doi.org/10.1016/j.coal.2015.05.009.
Yang, F., Xie, C.J., Ning, Z.F., Krooss, B.M., 2016. High-pressure methane sorption on dry and moisture-equilibrated shales. Energy Fuel. 31 (1), 482–492. https://doi.org/10.1021/acs.energyfuels.6b02999.
Yin, L.L., Guo, S.B., 2019. Full-sized pore structure and fractal characteristics of marine-continental transitional shale: a case study in Qinshui Basin, north China. Acta Geol. Sin. Engl. 93 (3), 675–691. https://doi.org/10.1111/1755-6724.13856.
Zhang, M., Fu, X.H., Zhang, Q.H., Cheng, W.P., 2019. Research on the organic geochemical and mineral composition properties and its influence on pore structure of coal-measure shales in Yushe-Wuxiang Block, South Central Qinshui Basin, China. J. Petrol. Sci. Eng. 173, 1065–1079. https://doi.org/10.1016/j.petrol.2018.10.079.
Zhang, T.W., Ellis, G.S., Ruppel, S.C., Milliken, K., Yang, R.S., 2012. Effect of organic-matter type and thermal maturity on methane adsorption in shale-gas

systems. Org. Geochem. 47, 120–131. https://doi.org/10.1016/j.orggeochem.2012.03.012.
Zhou, S.W., Wang, H.Y., Xue, H.Q., Guo, W., Li, X.B., 2017a. Discussion on the supercritical adsorption mechanism of shale gas based on Ono-Kondo lattice model. Earth Sci. 42 (8), 1421–1430. https://doi.org/10.3799/dqkx.2017.543 (in Chinese).
Zhou, S.W., Wang, H.Y., Xue, H.Q., Guo, W., Li, X.B., 2017b. Supercritical methane adsorption on shale gas: mechanism and model. Chin. Sci. Bull. 62 (35), 4189–4200. https://doi.org/10.1360/N972017-00151 (in Chinese).
Zhou, S.W., Xue, H.Q., Ning, Y., Guo, W., Zhang, Q., 2018. Experimental study of supercritical methane adsorption in Longmaxi shale: insights into the density of adsorbed methane. Fuel 211, 140–148. https://doi.org/10.1016/j.fuel.2017.09.065.